Competition of electron-phonon mediated superconductivity and Stoner magnetism on a flat band

Risto Ojajärvi,[1] Timo Hyart,[1,2] Mihail A. Silaev,[1] and Tero T. Heikkilä[1]
[1]*Department of Physics and Nanoscience Center, University of Jyvaskyla, P.O. Box 35 (YFL), FI-40014 Jyvaskyla, Finland*
[2]*Institut für Theoretische Physik, Universität Leipzig, D-04103 Leipzig, Germany*

(Received 7 March 2018; revised manuscript received 21 June 2018; published 22 August 2018)

The effective attractive interaction between electrons, mediated by electron-phonon coupling, is a well-established mechanism of conventional superconductivity. In metals exhibiting a Fermi surface, the critical temperature of superconductivity is exponentially smaller than the characteristic phonon energy. Therefore, such superconductors are found only at temperatures below a few kelvin. Systems with flat energy bands have been suggested to cure the problem and provide a route to room-temperature superconductivity, but previous studies are limited to only BCS models with an effective attractive interaction. Here we generalize Eliashberg's theory of strong-coupling superconductivity to systems with flat bands and relate the mean-field critical temperature to the microscopic parameters describing electron-phonon and electron-electron interaction. We also analyze the strong-coupling corrections to the BCS results and construct the phase diagram exhibiting superconductivity and magnetic phases on an equal footing. Our results are especially relevant for novel quantum materials where electronic dispersion and interaction strength are controllable.

DOI: 10.1103/PhysRevB.98.054515

I. INTRODUCTION

The overarching idea in quantum materials is to design the electronic (or optical, magnetic, etc.) properties of materials to perform the desired functionality [1]. This goal is aided by generic models and concepts, such as specific lattice models that lead to certain topological phases. Often the studied models and the resulting topological phases for electronic systems are noninteracting and do not include the possibility of spontaneous symmetry breaking. However, such noninteracting models are platforms for exotic electron dispersions that provide a basis for studying symmetry-broken interacting phases. In particular, certain models support approximate flat bands [2–10], and here we consider microscopic mechanisms for symmetry-breaking phases in such systems.

We analyze the interplay of electron-phonon [11] and (screened) electron-electron interaction in providing means for a symmetry-broken phase transition, thereby coupling together works on flat-band superconductivity [2,7,10,12] with those on flat-band (Stoner) magnetism [9,13–17]. In both cases the resulting mean-field critical temperature is linearly proportional to the coupling constant [18], thus allowing for a very high critical temperature. The two types of interaction mechanisms work in opposite directions and, in the case of weak interactions, in a symmetric way. However, upon increasing the coupling strength the retarded nature of the electron-phonon interaction shows up (as opposed to the instantaneous electron-electron interaction), breaking the symmetry between the two. In particular, we generalize Eliashberg's strong-coupling theory of superconductivity [19], usually formulated for systems with a Fermi surface, for flat bands. As a result, we describe the dimensionless BCS attractive interaction [20] in terms of the electron-phonon coupling and the characteristic phonon frequency [Eq. (8)]. In addition, we provide the generalization of the well-known McMillan formula of strong-coupling superconductivity (for Fermi surface systems) [21] to the case with flat bands in Eq. (14).

In addition to superconductivity, we consider flat-band Stoner magnetism. Because of the retarded nature of the electron-phonon interaction, the combined interaction can simultaneously have attractive and repulsive components, and thus the system can be unstable with respect to both singlet superconductivity and magnetism (see a generic strong-coupling phase diagram in Fig. 1). Often one of the phases still dominates and suppresses the other, but we find that when the critical temperatures of the phases are similar, both phases are local minima of the free energy at low temperatures. We find that their bulk coexistence and the resulting odd-frequency triplet superconducting order [22,23] are only realized as an unstable solution. On the other hand, these phases can form metastable domains inside the sample, and therefore an odd-frequency triplet order parameter can appear at the domain walls.

The structure of this paper is as follows. In Sec. II we introduce the model of surface bands with electron-phonon and Coulomb interactions. In Sec. III we formulate the Eliashberg model extension for the surface bands, describe all possible ordered states that can appear within this model, and calculate the critical temperatures of the superconducting and antiferromagnetic states. We study the competition and possible coexistence of these two types of ordering in Sec. IV. Conclusions are given in Sec. V.

II. MODEL

As a low-energy model for the flat band, we assume two sublattices coupled through an electronic Hamiltonian [3]

$$H_{\mathrm{el},p} = \begin{pmatrix} 0 & \varepsilon_p \\ \varepsilon_p & 0 \end{pmatrix}, \quad \text{with } \varepsilon_p = \varepsilon_0 \left(\frac{p}{p_{\mathrm{FB}}} \right)^N, \qquad (1)$$

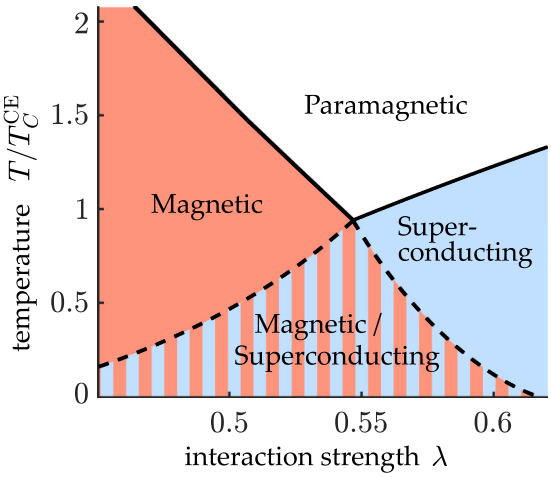

FIG. 1. Strong-coupling phase diagram for flat-band systems as a function of electron-phonon attraction λ for electron-electron repulsion $u = 0.5\omega_E$ [Eq. (8)]. T_C^{CE} is the temperature at which the T_C's of magnetic and superconducting order coincide. In the striped region these phases can form metastable domains inside the sample. This diagram is for $N \to \infty$. For finite N the overlap region between the phases is smaller.

where an integer N parametrizes the flatness of the dispersion, and ε_0 is the energy at $p = p_{\mathrm{FB}}$. The model is electron-hole symmetric and the two energy bands have the dispersions $\pm\varepsilon_p$. For large N, the states with low momenta, $|\mathbf{p}| < p_{\mathrm{FB}}$, are almost at zero energy and the density of states is very high. The states with momenta larger than p_{FB} do not contribute much to the momentum integrals due to their low density of states. Therefore, the results for large N do not depend much on the momentum cutoff, as long as it is larger than p_{FB}. In our model we take the cutoff to infinity and consider only the cases $N > 2$. This is in contrast to models with isolated flat bands extending throughout the Brillouin zone. The effects discussed below in the case of large N are mostly applicable also to such models (provided they have the type of sublattice degree of freedom discussed below), as long as p_{FB} is taken as the size of the Brillouin zone. Equation (1) is approximately realized for the surface states of N-layer rhombohedrally stacked graphite. In that system the surface states delocalize into the bulk at the edges of the flat band and this gives a momentum-dependent correction in the low-energy Hamiltonian [12,24]. In the case of $N \to \infty$ the delocalization of the surface states to the bulk leads to strong amplitude mode fluctuations invalidating the mean-field theory [24]. Therefore, the theory considered in this paper is applicable to rhombohedral graphite only in the case where N is not too large.

We model the electron-electron interaction as a repulsive on-site Hubbard interaction [25] with energy U. The magnitude of U depends on the microscopic details of the system and its environment. The coupling between electrons and phonons, with strength g, creates an effective attraction between the electrons and makes the system susceptible to superconductivity [19]. We mostly consider Einstein phonons with constant energy $\omega_q = \omega_E$ and discuss generalizations in the Supplemental Material [26].

The total Hamiltonian incorporating these effects is

$$H = \sum_{p,\sigma} \Psi^\dagger_{p\sigma} H_{\mathrm{el},p} \Psi_{p,\sigma} + \sum_{q,\rho} \omega_q b^\dagger_{q,\rho} b_{q,\rho} + \frac{U}{2\mathcal{N}} \sum_{\substack{p,k,q \\ \rho,\sigma,\sigma\prime}} \psi^\dagger_{p+q,\sigma\rho} \psi^\dagger_{k-q,\sigma'\rho} \psi_{k,\sigma'\rho} \psi_{p,\sigma\rho} + \frac{g}{\sqrt{\mathcal{N}}} \sum_{p,q,\sigma,\rho} (b^\dagger_{-q,\rho} + b_{q,\rho}) \psi^\dagger_{p+q,\sigma\rho} \psi_{p,\sigma\rho}, \tag{2}$$

where $\mathcal{N}$ is the number of lattice points in the system and $\Psi^\dagger_{p\sigma} = (\psi^\dagger_{p\sigma A}, \psi^\dagger_{p\sigma B})$ is a pseudospinor in sublattice space. We assume that the low-energy states on the two sublattices $\rho = A/B$ are spatially separated (e.g., localized on the two surfaces in rhombohedral graphite), so that neither the electron-electron interactions nor the phonons couple them. The only coupling between the sublattices comes from the off-diagonal dispersion relation. In the Supplemental Material we also show that the flat-band phenomenology applies to linear, graphenelike dispersion with an electronic Hamiltonian

$$H_{\mathrm{el},p} = v_{\mathrm{F}} \begin{pmatrix} 0 & p_x - ip_y \\ p_x + ip_y & 0 \end{pmatrix}, \tag{1'}$$

and with an energy cutoff ε_c and Fermi velocity v_F, provided the interaction energy scales are large compared to ε_c. Hence, our results may also apply as an effective model for twisted bilayer graphene close to its "magic" angles [30].

In the theory of electron-phonon superconductivity of metals, the neglect of higher-order diagrams in the perturbation theory is typically justified with the help of the Migdal theorem [31]. In that case, the expansion parameter gets an additional factor of ω_E/E_F, where E_F is the Fermi energy. Because of the Migdal theorem, the theory of superconductivity for metals is not strictly limited to weak coupling with respect to the interaction parameter.

In the flat band, however, the chemical potential is located at the bottom of the band and there is no Fermi energy with which to compare the Debye energy. Migdal's theorem cannot be used in this case. In the intermediate case of narrow electronic bands, corrections in the higher orders of the adiabatic parameter ω_E/E_F have been studied in Refs. [32–35] and the Eliashberg theory has been found also to be in agreement with Monte Carlo results in the weak-coupling regime when $\omega_E/E_F = 1$ in Ref. [36]. We find that the diagrams beyond the mean-field approximation do not influence the self-energies significantly if the effective pairing constant introduced below in Eq. (8) is small, $\lambda \ll 1$, and $\omega_E, u \ll \varepsilon_0$. Moreover, although the mean-field theory is applied beyond its formal limits of validity in the strong-coupling regime, this theory captures the interesting possibility that the retarded nature of the electron-phonon interaction can lead to the presence of attractive and repulsive components at the same time. As a result, the system can be simultaneously unstable with respect to the appearance of both singlet superconductivity and magnetism as discussed in Sec. IV.

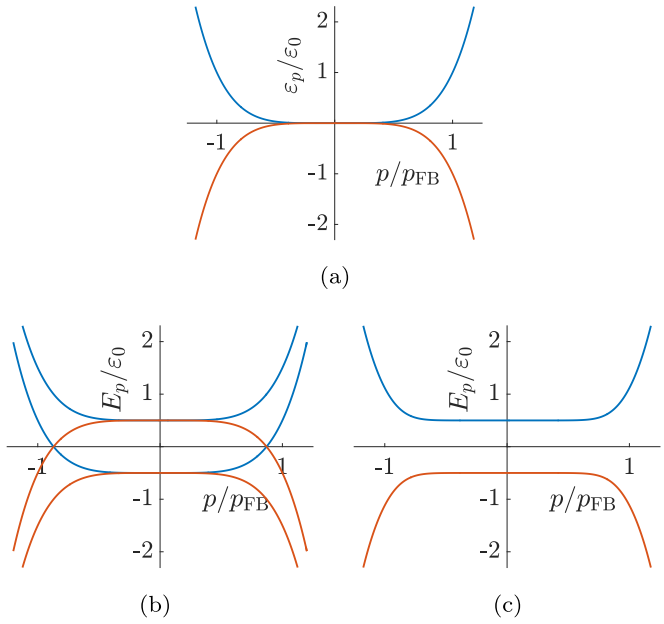

FIG. 2. Quasiparticle dispersions $E(p)$ for different kinds of symmetry breakings with $N = 5$. (a) In the noninteracting case, the spin bands are degenerate with $E(p) = \pm\varepsilon(p)$. (b) For the ferromagnetic (FM) or the superconducting (SC) phase with a $\theta = \pi$ phase shift between the sublattices, one quasiparticle band is shifted up and the other down in energy. In this case, no energy gap is opened. (c) For the antiferromagnetic (AFM) or the SC phase with $\theta = 0$ an energy gap is opened and quasiparticle bands are doubly degenerate.

III. ORDERED STATES

Hamiltonian (2) allows for a number of spontaneous symmetry-breaking phases. We restrict our study to spatially homogeneous phases. Therefore, the order parameter can appear in the spin, sublattice (pseudospin), and electron-hole (Nambu) spaces. The general self-energy is

$$\Sigma(i\omega_n) = \sum_{i,j,k=0}^{3} \Sigma_{ijk}(i\omega_n)\tau_i\sigma_j\rho_k, \tag{3}$$

where τ_i, σ_j, and ρ_k are the Pauli matrices in electron-hole, spin, and sublattice spaces, respectively. We characterize the different components Σ_{ijk} and determine their values within the self-consistent Hartree-Fock model. This reduces to solving a set of nonlinear integral equations, known as Eliashberg equations in the context of conventional superconductors.

To explore the possible phases of the system, we first assume that the $U(1)$ gauge symmetry is broken, but the $SU(2)$ spin-rotation symmetry is not. After fixing the overall phase of the superconducting order parameter, we are left with the self-energy $\Sigma_{000}(i\omega_n)$ and three degrees of freedom for the superconducting singlet order parameter: the magnitudes of the order parameter on the sublattices Δ_A and Δ_B and the relative phase θ. Choosing $\theta = 0$ leads to a gapped quasiparticle dispersion [Fig. 2(c)], whereas $\theta = \pi$ would imply a gapless dispersion [Fig. 2(b)]. Thus, in the case of an instantaneous interaction the total energy is minimized when $\theta = 0$ and $\Delta_A = \Delta_B$. Generalizing the above to the frequency-dependent interactions, we choose the singlet to be proportional to the $\tau_2\sigma_2\rho_0$ component, whose magnitude and the functional form are obtained from the self-consistency equation. The self-energy for the fermionic Matsubara frequency ω_n is

$$\Sigma_{\mathrm{SC}}(i\omega_n) = -i\,\Sigma_n^{\omega}\mathbb{1} + \phi_n\tau_2\sigma_2, \tag{4}$$

where $\Sigma_n^{\omega} = (1 - Z_n)\omega_n$ is the frequency renormalization by the retarded interaction [19]. To simplify the equations, we define renormalized frequencies $\tilde{\omega}_n = Z_n\omega_n$. We use the symbol ϕ_n for the "bare" singlet order parameter and Δ for the maximum value of the renormalized singlet order parameter $\Delta_n \equiv \phi_n/Z_n$ related to the energy gap.

When $SU(2)$ spin-rotation symmetry is broken but $U(1)$ gauge symmetry is not, the self-energies describe the frequency renormalization and the magnetization. After fixing the direction of the magnetization on one sublattice, the relevant degrees of freedom are reduced to three similarly as in the superconducting case. These can be chosen as the magnitudes of the magnetizations in the two sublattices h_A and h_B and the relative angle φ between their directions. The quasiparticle dispersion in the magnetic case is the same as in the superconducting case if we identify $\Delta_{A,B} = h_{A,B}$ and $\theta = \pi - \varphi$ (see Fig. 2). In this case, the relative angle $\varphi = 0$ leads to a gapless quasiparticle dispersion [Fig. 2(b)], and $\varphi = \pi$ to a gapped dispersion [Fig. 2(c)]. Thus, the energy minimum is obtained with $h_A = h_B$ and $\varphi = \pi$. The stable magnetization is hence antiferromagnetic, with opposite magnetizations on the two sublattices, so that the self-energy is

$$\Sigma_{\mathrm{AFM}}(i\omega_n) = -i\,\Sigma_n^{\omega}\mathbb{1} + h_n\tau_3\sigma_3\rho_3, \tag{5}$$

where h_n is the frequency-dependent exchange field. This result agrees with density functional theory (DFT) studies on rhombohedral graphite [37], and similar magnetization structure has been predicted also in the case of flat bands appearing at the zigzag edges of graphene nanoribbons [38–40]. We also note that the AFM state is insulating [see Fig. 2(c)]. If the noninteracting dispersion is completely flat at zero energy, the sublattices are uncoupled and the antiferromagnetic state is degenerate with the ferromagnetic $\varphi = 0$ state.

By calculating the Hartree-Fock self-energies, we find the self-consistency equations, from which we can determine the values of the self-energy terms. For the superconducting (SC) self-energy (4), they are

$$\phi_n = 2T\sum_{m=-\infty}^{\infty}(\lambda_{nm} - u)\int_0^{\infty}\frac{dp\,p}{p_{\mathrm{FB}}^2}\frac{\phi_m}{\tilde{\omega}_m^2 + \varepsilon_p^2 + \phi_m^2}, \tag{6}$$

$$Z_n = 1 + 2T\sum_{m=-\infty}^{\infty}\lambda_{nm}\frac{\omega_m}{\omega_n}\int_0^{\infty}\frac{dp\,p}{p_{\mathrm{FB}}^2}\frac{Z_m}{\tilde{\omega}_m^2 + \varepsilon_p^2 + \phi_m^2}, \tag{7}$$

where the interaction kernel is $\lambda_{nm} = \lambda\omega_E^3/[\omega_E^2 + (\omega_n - \omega_m)^2]$. The functional form of the interaction kernel is determined by the phonon propagator from which it is derived. The width in frequency space is determined by the characteristic phonon frequency, which in this case is the Einstein frequency ω_E. The effective interaction constants in the flat band are

$$\lambda = \frac{g^2}{\omega_E^2}\frac{\Omega_{\mathrm{FB}}}{\Omega_{\mathrm{BZ}}}, \quad u = \frac{U\Omega_{\mathrm{FB}}}{\Omega_{\mathrm{BZ}}}, \tag{8}$$

where $\Omega_{\rm FB}$ and $\Omega_{\rm BZ}$ are the momentum-space areas of the flat band and of the first Brillouin zone, respectively.

For an antiferromagnet with self-energy (5), the self-consistency equations are

$$h_n = 2T\sum_{m=-\infty}^{\infty}(u-\lambda_{nm})\int_0^\infty \frac{dp\,p}{p_{\rm FB}^2}\frac{h_m}{\tilde{\omega}_m^2+\varepsilon_p^2+h_m^2}, \quad (9)$$

$$Z_n = 1+2T\sum_{m=-\infty}^{\infty}\lambda_{nm}\frac{\omega_m}{\omega_n}\int_0^\infty \frac{dp\,p}{p_{\rm FB}^2}\frac{Z_m}{\tilde{\omega}_m^2+\varepsilon_p^2+h_m^2}. \quad (10)$$

Superconductivity and magnetism are thus symmetric with each other also on the level of the self-consistency equations, but with the roles of u and λ_{nm} switched. Tovmasyan *et al.* have shown that this duality is also broken by taking into account higher-order terms in the perturbation theory [41].

To solve the self-consistency equations (6)–(10), we truncate the Matsubara sums with a cutoff $\omega_C \sim 10\omega_E$. This causes no numerical error if we use the pseudopotential trick and simultaneously replace u with an effective value u^*, which depends on the cutoff [42]. For superconductivity (magnetism), cutting off high-energy scatterings is compensated by a reduction (increase) in the low-energy effective interaction.

After the pseudopotential trick, the solutions are found by a fixed-point iteration. The iteration is continued until all of the components have converged. The fixed-point method only finds the stable solutions; to find the unstable solutions, we used a solver based on Newton's method.

The number of parameters in Eqs. (6)–(10) can be reduced by defining new interaction constants $\tilde{\lambda} \equiv \lambda(\omega_E/\varepsilon_0)^{2/N}$ and $\tilde{u} = u\omega_E^{2/N-1}/\varepsilon^{2/N}$, so that one parameter is eliminated completely and the results become proportional to ω_E.

For weak coupling, $\lambda \ll 1$, the frequency dependence of λ_{nm} can be disregarded and we can approximate $Z \approx 1$ and $\Delta \approx \phi$. Assuming $\lambda\omega_E > u$, the superconducting gap at $T = 0$ and the critical temperature are

$$\frac{\Delta_0}{\omega_E} = \frac{1}{2}\left[\frac{(\tilde{\lambda}-\tilde{u})\sqrt{\pi}\,\Gamma\left(\frac{1}{2}-\frac{1}{N}\right)}{N\sin\left(\frac{\pi}{N}\right)\Gamma\left(1-\frac{1}{N}\right)}\right]^{\frac{N}{N-2}}, \quad (11)$$

$$\frac{T_C^{\rm sc}}{\omega_E} = \frac{1}{2\pi}\left[\frac{(\tilde{\lambda}-\tilde{u})\zeta\left(2-\frac{2}{N}\right)\left(2^{2-\frac{2}{N}}-1\right)}{N\sin\left(\frac{\pi}{N}\right)}\right]^{\frac{N}{N-2}}. \quad (12)$$

These results are valid for $N > 2$ as the momentum integrals diverge without a cutoff for $N \leqslant 2$. Note that the $T = 0$ limit can thus be taken before the flat-band limit of large N. Analogous results have been obtained before within the BCS model in Ref. [12]. For large N, Δ_0 is linear in the coupling and its magnitude is proportional to the phonon energy scale. Hence the associated critical temperature can be very large. Relabeling $\Delta_0 \to h_0$ and $\tilde{\lambda} \leftrightarrow \tilde{u}$, we find similar equations for magnetism. Here h_0 is the magnetic order parameter at $T = 0$.

At strong coupling, the retardation matters and the results for magnetism and superconductivity diverge from each other. For superconductivity, we can improve on the weak-coupling result by including some of the corrections from the Eliashberg theory when $N\to\infty$. We still neglect the full frequency dependence, but we include the electron mass renormalization as a static factor $Z_0 = 1+\lambda$. The order parameter at zero temperature becomes

$$\Delta_0 = \frac{\lambda\omega_E - u}{2(1+2\lambda)}. \quad (13)$$

In metals with a Fermi surface [43], the electron-phonon interaction renormalizes the pairing potential with the factor of $1+\lambda$ instead of $1+2\lambda$ as in Eq. (13). Thus, for weak coupling, the electron-phonon renormalization is more effective in the flat band than in the usual metals. This difference is more pronounced at strong coupling, as we see next.

By linearizing Eqs. (6) and (7) with respect to ϕ, we can solve for the critical temperature [see Fig. 3(a)]. We find that when $N \to \infty$, the critical temperature scales as $T_C^{\rm sc} \propto \lambda^{0.2}\omega_E$ for large λ. In metals [43] the asymptotic scaling goes as $T_C^{\rm sc} \propto \lambda^{1/2}\omega_E$.

When $u \neq 0$, there is a critical point λ_C such that for $\lambda < \lambda_C$ there is no superconducting transition at any temperature. For small u/ω_E, λ_C is linearly proportional to the Coulomb interaction. For large u, λ_C increases sublinearly [see Fig. 3(b)].

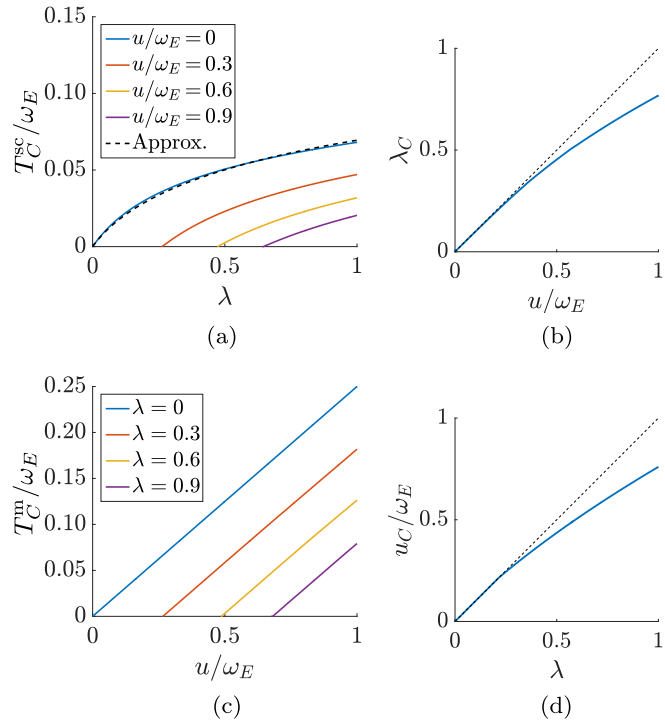

FIG. 3. Critical temperatures for superconducting and magnetic phases for $N \to \infty$. (a) Superconductivity is suppressed when $\lambda \lesssim u/\omega_E$. Above the critical point $\lambda_C(u)$, $T_C^{\rm sc}$ is linear in λ. With increasing λ, the electron-phonon renormalization increases and this limits the critical temperature. The dashed line is the approximation in Eq. (14). (b) Critical interaction strength for superconductivity as a function of u. When $\lambda < \lambda_C(u)$, superconductivity is suppressed. The dashed line is the instantaneous approximation. (c) Magnetism is suppressed when $u/\omega_E \lesssim \lambda$. Above the critical point $u_C(\lambda)$, $T_C^{\rm m}$ is linear in u. (d) Critical interaction strength for magnetism as a function of electron-phonon interaction. When $u < u_C(\lambda)$, magnetism is suppressed. The dashed line is the instantaneous approximation. In this figure, we do not take into account the possible magnetic instability of the superconducting state, or vice versa.

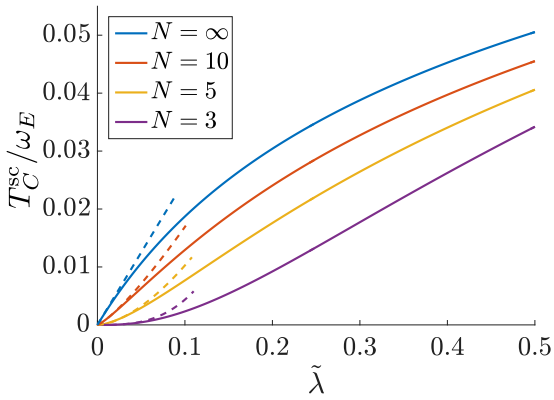

FIG. 4. Effect of finite N on critical temperature when $u = 0$. For small $\tilde{\lambda}$, the results coincide with the instantaneous approximation of Eq. (12) (shown with the dashed lines). For large $\tilde{\lambda}$, the strong-coupling corrections limit the increase in T_C^{sc}.

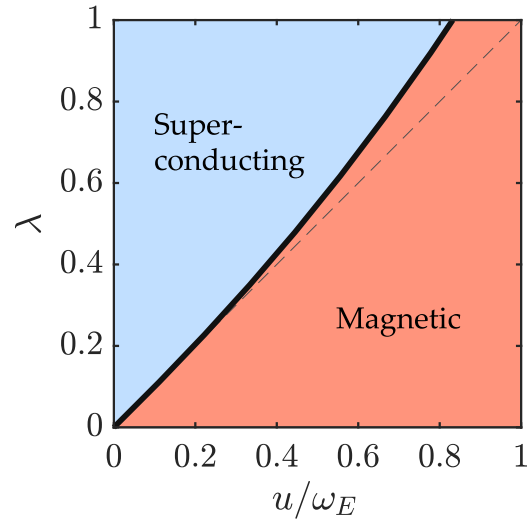

FIG. 5. Mean-field phase diagram for $N = \infty$ obtained by determining the line on which the critical temperatures for superconductivity and antiferromagnetism are equal. The thin dashed line shows the phase boundary $\lambda = u/\omega_E$ in the case of instantaneous interactions. When the energy scales of interactions are small compared to ω_E we recover the BCS results. The phase diagram for finite N looks similar but the retardation effects are weaker, so that the deviation from the BCS approximation is smaller.

An approximate numerical equation for T_C^{sc} is

$$T_C^{sc} = \frac{\lambda\omega_E - u(1 - 0.3u/\omega_E)}{4(1 + 2.6\lambda^{0.8})}. \tag{14}$$

This is a flat-band analog of the McMillan equation [21], which for the conventional superconductors incorporates the Eliashberg and Coulomb corrections to T_C^{sc}. The u^2 term in the numerator accounts for the retardation correction to λ_C as in Fig. 3(b). The form of the denominator is chosen to show the $\lambda^{0.2}$ power-law behavior for large λ. The factor 2.6 is obtained by a fit in the region $\lambda < 1$ for $u = 0$. The fit is shown as the dashed line in Fig. 3(a).

The ratio Δ_0/T_C^{sc} is not constant, but depends on both N and λ. For $N \to \infty$, the ratio has the value 2 for weak coupling and increases as λ increases. For $\lambda = 1$ the ratio is 2.56. For the critical temperature at finite N, see Fig. 4.

The phenomenology of the magnetism can be understood as follows. According to the Stoner criterion, the magnetization is related to the competition between the exchange energy gain and the kinetic energy penalty from moving electrons from one spin band to another. For a flat band with $N \to \infty$, there is no kinetic energy penalty, and at zero temperature with $\lambda = 0$ even a small exchange interaction leads to a complete magnetization of the flat band. In the presence of the electron-phonon interaction the competition is between the exchange energy gain and the electron-phonon energy penalty, which coincide at $u = u_C$. If we can neglect the retardation, the total interaction in Eq. (9) is $u - \lambda\omega_E$. The flat band is completely magnetized when $u > u_C \approx \lambda\omega_E$. Due to retardation, for large λ the critical point is reduced from the linear estimate [see Fig. 3(d)].

Above, we have discussed the superconducting order parameter ϕ. The other important property of the superconducting state is the existence of a supercurrent. In the flat band the electronic group velocity vanishes and it is not immediately clear that there can be a finite supercurrent. However, the flat-band surface states of superconducting rhombohedral graphite do support a finite supercurrent [44] and similarly it is known that quantum Hall pseudospin ferromagnets can support a finite pseudospin supercurrent [16]. More generally, Peotta and Törmä [7] have shown that for a topological flat band there is an additional geometric contribution to the superfluid weight so that the critical current is finite. As we have not fixed the underlying topology in our model, it can be applied to topologically nontrivial flat bands.

As one can see, the Eliashberg model describes the nucleation of both the magnetic and superconducting phases which can have rather close critical temperatures as shown in Fig. 3. In the next section we consider the nonlinear problem by calculating the entire phase diagram of the ordered states to study the competition and the possible coexistence between the superconductivity and antiferromagnetism.

IV. COMPETITION BETWEEN THE PHASES

If the electron-phonon interaction is approximated as instantaneous, we can sum the two interactions together and have either a total interaction, which makes the normal state unstable to the superconducting transition ($\lambda\omega_E - u > 0$) or to the magnetic transition ($\lambda\omega_E - u < 0$), but not to both at once. On the other hand, if the electron-phonon interaction is retarded, the situation is different, as the total interaction can be attractive for low frequencies but repulsive for high frequencies. There is then a parameter range in which both phases are local minima of the free energy. This occurs when λ is large enough to overcome the suppressing effect of u in the case of superconductivity [$\lambda > \lambda_C(u)$ in Fig. 3(b)], but at the same time u is large enough to overcome the suppressing effect of λ and create a magnetic instability [$u > u_C(\lambda)$ in Fig. 3(d)].

We study the phase diagram of the system by determining the state with a higher critical temperature as a function of u and λ (Fig. 5). The phase diagram is almost symmetric with respect to SC and AFM phases except that the lack of retardation in

electron-electron repulsion favors the AFM phase for strong coupling.

Even if there is a parameter region in T, u, and λ where both SC and AFM self-consistency equations have a finite solution, it does not mean that both phases are necessarily simultaneously present. To determine the stability, we construct the coupled self-consistency equations in the case when both order parameters are nonzero and interact with each other [26]. By linearizing the coupled self-consistency equation with respect to SC, and solving the AFM part fully, the stability of the AFM phase with respect to the SC transition can be determined, and vice versa. Figure 1 shows the region in λ-T space with fixed u, where the two phases are stable. The figure shows that in the region where SC is dominant, the AFM phase is unstable near the expected second-order transition (the solid line between the magnetic and paramagnetic phases) but becomes a local minimum of free energy at lower temperatures. The same happens for superconductivity when the AFM phase dominates. The transition between SC and AFM phases is of the first order.

When discussing superconductivity in the presence of an exchange field (either induced or spontaneous), we have an additional ingredient in the self-energy, namely, the superconducting triplet order parameter [22,45], which has been discussed in the context of the Eliashberg model in Ref. [46]. The triplet is spatially isotropic, and in order to satisfy the fermionic antisymmetry, it has to be odd in frequency. It is generated in the self-energy only when there is an odd-frequency component in the interaction. In the retarded interaction, this is always satisfied. When calculating the stability of the AFM phase with respect to SC, the triplet appears in the linear order. It hence modifies the boundaries of the region where both AFM and SC phases are stable. We have taken this effect into account in Fig. 1.

Besides the competition between AFM and SC phases, we need to consider the possibility of a coexistence phase in the dashed region of Fig. 1, where both phases can show up alone. We indeed have numerically found such a coexistence solution, but tests based on fixed-point iteration revealed it to be unstable at every temperature that we checked. This finding is in accordance with a simplified model where both interaction channels are instantaneous and independent of each other [26].

However, the fact that the two phases are simultaneously local minima of the free energy suggests that this system could have domains of antiferromagnetic order coexisting with superconducting domains. Such domains would be separated by a domain wall mixing the two kinds of phases and inducing odd-frequency triplet pairing, as schematically illustrated in Fig. 6. In addition to providing a mechanism for the appearance of odd-frequency triplet pairing, the domain walls can support interesting excitations. In particular, it is known that flat-band ferromagnets can support interesting topological and domain-wall excitations in the form of different kinds of spin textures [16,47], and various combinations of spin textures and superconductivity may lead to the appearance of Majorana zero modes [48–52]. Also, alternatively to the intrinsic domain structure generation, the ferromagnetic superconductors can support different types of nonuniform magnetic order and spontaneous vortex states [53–55]. A detailed analysis of different possibilities goes beyond the scope of this paper.

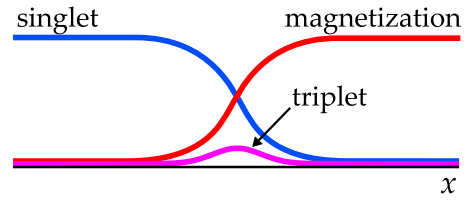

FIG. 6. Sketch of a domain wall between magnetic (red) and superconducting (blue) domains. At the domain wall a triplet component (purple) is induced.

V. CONCLUSIONS

We have proposed a simplified model of a flat-band system with a retarded electron-phonon interaction and a repulsive Hubbard interaction. For this model, we have determined the self-consistency equations in the Hartree-Fock approximation and all the possible homogeneous phases. Antiferromagnetism and superconductivity are essentially symmetric in this system, with the only difference coming from the retardation of the electron-phonon interaction. For large λ, the retardation suppresses the increase in Δ more effectively in a flat band than in metals with a Fermi surface. We find that the retardation also creates a situation in which both phases are separately local minima of the free energy, suggesting a possibility of coexisting antiferromagnetic and superconducting domains inside the sample.

Our results indicate how flat-band superconductivity can be generated from electron-phonon interaction and provides means to estimate the mean-field critical temperature when the details of the electron-phonon coupling and the screened interaction are known. The superfluid transition in low-dimensional systems occurs in the form of a Berezinskii-Kosterlitz-Thouless (BKT) transition at a temperature that is lower than the mean-field transition temperature. That the latter is nonzero is ensured by the possibility of having a nonvanishing supercurrent (see, for example, Refs. [7,10,44]) in a flat-band superconductor. Our results are of relevance in designing novel types of quantum materials for the interplay of superconducting and magnetic order, and the search for systems exhibiting exotic superconductivity with a very high critical temperature, up to room temperature. They may also shed light on recent evidence of high-temperature superconductivity in graphite interfaces [56].

Our results could also explain some of the phenomena associated with the recent experiments on bilayer graphene [30,57]. (For a more microscopic description of that case within the BCS model, see Refs. [58,59].) In the experiment, the twist angle between two superimposed graphene layers is chosen to a certain magic angle, so that the two Dirac cones in the graphene layers hybridize, forming a pair of flat bands. Our model can be adjusted to describe this situation with small changes (see the Supplemental Material [26] for details). When the chemical potential was tuned to the lower of these bands, the system became an insulator. From our point of view, this could be the insulating AFM state we describe. When the chemical potential is tuned slightly off from the flat band, a superconducting dome in the T-μ phase diagram was observed on both sides. These domes can be the s-wave SC phases

we describe here. The competition between the particle-hole (AFM) and the particle-particle (SC) channels in the presence of the chemical potential was considered by Löthman and Black-Schaffer in Ref. [8], and for a range of parameters, they reproduce a similar phase diagram near the flat band, with the AFM state at the level of the flat band and two superconducting domes with doping away from the flat band (see Fig. 2(b) in Ref. [8]). In the experiments, SC domes are only observed on the hole-doped side. The electron-doped side exhibits only insulating behavior near the flat band. One possible explanation is the difference in screening, which changes the relative magnitude of the repulsive and attractive interactions, so that the AFM state covers the SC domes completely. However, we leave the detailed treatment of the effects of doping and screening (both intrinsic and that provided by the environment) for further work.

ACKNOWLEDGMENTS

We thank Sebastiano Peotta, Long Liang, and Päivi Törmä for helpful comments. This project was supported by the Academy of Finland Key Funding (Project No. 305256), Center of Excellence (Project No. 284594), and Research Fellow (Project No. 297439) programs.

[1] B. Keimer and J. E. Moore, The physics of quantum materials, Nat. Phys. **13**, 1045 (2017).
[2] V. A. Shaginyan and V. R. Khodel, Superfluidity in system with fermion condensate, JETP Lett. **51**, 553 (1990).
[3] T. T. Heikkilä, N. B. Kopnin, and G. E. Volovik, Flat bands in topological media, JETP Lett. **94**, 233 (2011).
[4] T. T. Heikkilä and G. E. Volovik, *Basic Physics of Functionalized Graphite* (Springer, Berlin, 2016), Chap. 6.
[5] E. Tang and L. Fu, Strain-induced partially flat band, helical snake states and interface superconductivity in topological crystalline insulators, Nat. Phys. **10**, 964 (2014).
[6] S. Matsuura, P.-Y. Chang, A. P. Schnyder, and S. Ryu, Protected boundary states in gapless topological phases, New J. Phys. **15**, 065001 (2013).
[7] S. Peotta and P. Törmä, Superfluidity in topologically nontrivial flat bands, Nat. Commun. **6**, 8944 (2015).
[8] T. Löthman and A. M. Black-Schaffer, Universal phase diagrams with superconducting domes for electronic flat bands, Phys. Rev. B **96**, 064505 (2017).
[9] E. H. Lieb, Two Theorems on the Hubbard Model, Phys. Rev. Lett. **62**, 1201 (1989).
[10] V. J. Kauppila, F. Aikebaier, and T. T. Heikkilä, Flat-band superconductivity in strained Dirac materials, Phys. Rev. B **93**, 214505 (2016).
[11] H. Fröhlich, Theory of the superconducting state. I. The ground state at the absolute zero of temperature, Phys. Rev. **79**, 845 (1950).
[12] N. B. Kopnin, T. T. Heikkilä, and G. E. Volovik, High-temperature surface superconductivity in topological flat-band systems, Phys. Rev. B **83**, 220503 (2011).
[13] H. Tasaki, Ferromagnetism in the Hubbard Models with Degenerate Single-Electron Ground States, Phys. Rev. Lett. **69**, 1608 (1992).
[14] A. Mielke and H. Tasaki, Ferromagnetism in the Hubbard model, Commun. Math. Phys. **158**, 341 (1993).
[15] O. Derzhko, A. Honecker, and J. Richter, Low-temperature thermodynamics for a flat-band ferromagnet: Rigorous versus numerical results, Phys. Rev. B **76**, 220402 (2007).
[16] K. Moon, H. Mori, K. Yang, S. M. Girvin, A. H. MacDonald, L. Zheng, D. Yoshioka, and S.-C. Zhang, Spontaneous interlayer coherence in double-layer quantum Hall systems: Charged vortices and Kosterlitz-Thouless phase transitions, Phys. Rev. B **51**, 5138 (1995).
[17] H. A. Fertig, Energy spectrum of a layered system in a strong magnetic field, Phys. Rev. B **40**, 1087 (1989).
[18] S. T. Belyaev, On the nature of the first excited states of even-even spherical nuclei, Sov. Phys. JETP **12**, 968 (1961).
[19] G. M. Eliashberg, Interactions between electrons and lattice vibrations in a superconductor, Sov. Phys. JETP **11**, 696 (1960).
[20] J. Bardeen, L. N. Cooper, and J. R. Schrieffer, Theory of superconductivity, Phys. Rev. **108**, 1175 (1957).
[21] W. L. McMillan, Transition temperature of strong-coupled superconductors, Phys. Rev. **167**, 331 (1968).
[22] V. L. Berezinskii, New model of the anisotropic phase of superfluid He-3, JETP Lett. **20**, 287 (1974).
[23] M. Matsumoto, M. Koga, and H. Kusunose, Coexistence of even- and odd-frequency superconductivities under broken time-reversal symmetry, J. Phys. Soc. Jpn. **81**, 033702 (2012).
[24] V. J. Kauppila, T. Hyart, and T. T. Heikkilä, Collective amplitude mode fluctuations in a flat band superconductor formed at a semimetal surface, Phys. Rev. B **93**, 024505 (2016).
[25] J. Hubbard, Electron correlations in narrow energy bands, Proc. R. Soc. London, Ser. A **276**, 238 (1963).
[26] See Supplemental Material at http://link.aps.org/supplemental/10.1103/PhysRevB.98.054515 for more details. In addition to the references in the main paper, the Supplemental Information includes Refs. [27–29].
[27] J. M. B. Lopes do Santos, N. M. R. Peres, and A. H. Castro Neto, Continuum model of the twisted graphene bilayer, Phys. Rev. B **86**, 155449 (2012).
[28] E. Suárez Morell, J. D. Correa, P. Vargas, M. Pacheco, and Z. Barticevic, Flat bands in slightly twisted bilayer graphene: Tight-binding calculations, Phys. Rev. B **82**, 121407 (2010).
[29] N. B. Kopnin and E. B. Sonin, BCS Superconductivity of Dirac Electrons in Graphene Layers, Phys. Rev. Lett. **100**, 246808 (2008).
[30] Y. Cao, V. Fatemi, S. Fang, K. Watanabe, T. Taniguchi, E. Kaxiras, and P. Jarillo-Herrero, Unconventional superconductivity in magic-angle graphene superlattices, Nature (London) **556**, 43 (2018).
[31] A. B. Migdal, Interaction between electrons and lattice vibrations in a normal metal, Sov. Phys. JETP **7**, 996 (1958).
[32] C. Grimaldi, L. Pietronero, and S. Strässler, Nonadiabatic Superconductivity: Electron-Phonon Interaction Beyond Migdal's Theorem, Phys. Rev. Lett. **75**, 1158 (1995).
[33] L. Pietronero, S. Strässler, and C. Grimaldi, Nonadiabatic superconductivity. I. Vertex corrections for the electron-phonon interactions, Phys. Rev. B **52**, 10516 (1995).
[34] C. Grimaldi, L. Pietronero, and S. Strässler, Nonadiabatic superconductivity. II. Generalized Eliashberg equations beyond Migdal's theorem, Phys. Rev. B **52**, 10530 (1995).

[35] M. Botti, E. Cappelluti, C. Grimaldi, and L. Pietronero, Nonadiabatic theory of the superconducting state, Phys. Rev. B **66**, 054532 (2002).

[36] I. Esterlis, B. Nosarzewski, E. W. Huang, B. Moritz, T. P. Devereaux, D. J. Scalapino, and S. A. Kivelson, Breakdown of Migdal-Eliashberg theory: A determinant quantum Monte Carlo study, Phys. Rev. B **97**, 140501 (2018).

[37] B. Pamuk, J. Baima, F. Mauri, and M. Calandra, Magnetic gap opening in rhombohedral-stacked multilayer graphene from first principles, Phys. Rev. B **95**, 075422 (2017).

[38] M. Fujita, K. Wakabayashi, K. Nakada, and K. Kusakabe, Peculiar localized state at zigzag graphite edge, J. Phys. Soc. Jpn. **65**, 1920 (1996).

[39] J. Fernández-Rossier, Prediction of hidden multiferroic order in graphene zigzag ribbons, Phys. Rev. B **77**, 075430 (2008).

[40] Y.-W. Son, M. L. Cohen, and S. G. Louie, Half-metallic graphene nanoribbons, Nature (London) **444**, 347 (2006).

[41] M. Tovmasyan, S. Peotta, P. Törmä, and S. D. Huber, Effective theory and emergent SU(2) symmetry in the flat bands of attractive Hubbard models, Phys. Rev. B **94**, 245149 (2016).

[42] P. Morel and P. W. Anderson, Calculation of the superconducting state parameters with retarded electron-phonon interaction, Phys. Rev. **125**, 1263 (1962).

[43] J. P. Carbotte, Properties of boson-exchange superconductors, Rev. Mod. Phys. **62**, 1027 (1990).

[44] N. B. Kopnin, Surface superconductivity in multilayered rhombohedral graphene: Supercurrent, JETP Lett. **94**, 81 (2011).

[45] A. Balatsky and E. Abrahams, New class of singlet superconductors which break the time reversal and parity, Phys. Rev. B **45**, 13125 (1992).

[46] H. Kusunose, M. Matsumoto, and M. Koga, Strong-coupling superconductivity with mixed even-and odd-frequency pairing, Phys. Rev. B **85**, 174528 (2012).

[47] D. I. Pikulin, P. G. Silvestrov, and T. Hyart, Confinement-deconfinement transition due to spontaneous symmetry breaking in quantum Hall bilayers, Nat. Commun. **7**, 10462 (2016).

[48] T.-P. Choy, J. M. Edge, A. R. Akhmerov, and C. W. J. Beenakker, Majorana fermions emerging from magnetic nanoparticles on a superconductor without spin-orbit coupling, Phys. Rev. B **84**, 195442 (2011).

[49] B. Braunecker and P. Simon, Interplay Between Classical Magnetic Moments and Superconductivity in Quantum One-Dimensional Conductors: Toward a Self-Sustained Topological Majorana Phase, Phys. Rev. Lett. **111**, 147202 (2013).

[50] J. Klinovaja, P. Stano, A. Yazdani, and D. Loss, Topological Superconductivity and Majorana Fermions in RKKY Systems, Phys. Rev. Lett. **111**, 186805 (2013).

[51] M. M. Vazifeh and M. Franz, Self-Organized Topological State with Majorana Fermions, Phys. Rev. Lett. **111**, 206802 (2013).

[52] F. Pientka, L. I. Glazman, and F. von Oppen, Topological superconducting phase in helical Shiba chains, Phys. Rev. B **88**, 155420 (2013).

[53] P. W. Anderson and H. Suhl, Spin alignment in the superconducting state, Phys. Rev. **116**, 898 (1959).

[54] L. N. Bulaevskii, A. I. Buzdin, M. L. Kulić, and S. V. Panjukov, Coexistence of superconductivity and magnetism theoretical predictions and experimental results, Adv. Phys. **34**, 175 (1985).

[55] L. Y. Vinnikov, I. S. Veshchunov, S. Y. Grebenchuk, D. S. Baranov, V. S. Stolyarov, V. V. Dremov, N. Zhou, Z. X. Shi, X. F. Xu, S. Pyon, Y. Sun, W. Jiao, G. Cao, A. A. Golubov, D. Roditchev, A. I. Buzdin, and T. Tamegai, Direct evidence of spontaneous Abrikosov vortex state in ferromagnetic superconductor $EuFe_2(As_{1-x}P_x)_2$ with $x = 0.21$, arXiv:1709.09802.

[56] C. E. Precker, P. D. Esquinazi, A. Champi, J. Barzola-Quiquia, M. Zoraghi, S. Muios-Landin, A. Setzer, W. Bühlmann, D. Spemann, J. Meijer, T. Muenster, O. Baehre, G. Kloess, and H. Beth, Identification of a possible superconducting transition above room temperature in natural graphite crystals, New J. Phys. **18**, 113041 (2016).

[57] Y. Cao, V. Fatemi, A. Demir, S. Fang, S. L. Tomarken, J. Y. Luo, J. D. Sanchez-Yamagishi, K. Watanabe, T. Taniguchi, E. Kaxiras, R. C. Ashoori, and P. Jarillo-Herrero, Correlated insulator behaviour at half-filling in magic-angle graphene superlattices, Nature (London) **556**, 80 (2018).

[58] T. J. Peltonen, R. Ojajärvi, and T. T. Heikkilä, Mean-field theory for superconductivity in twisted bilayer graphene, arXiv:1805.01039.

[59] F. Wu, A. H. MacDonald, and I. Martin, Theory of phonon-mediated superconductivity in twisted bilayer graphene, arXiv:1805.08735.